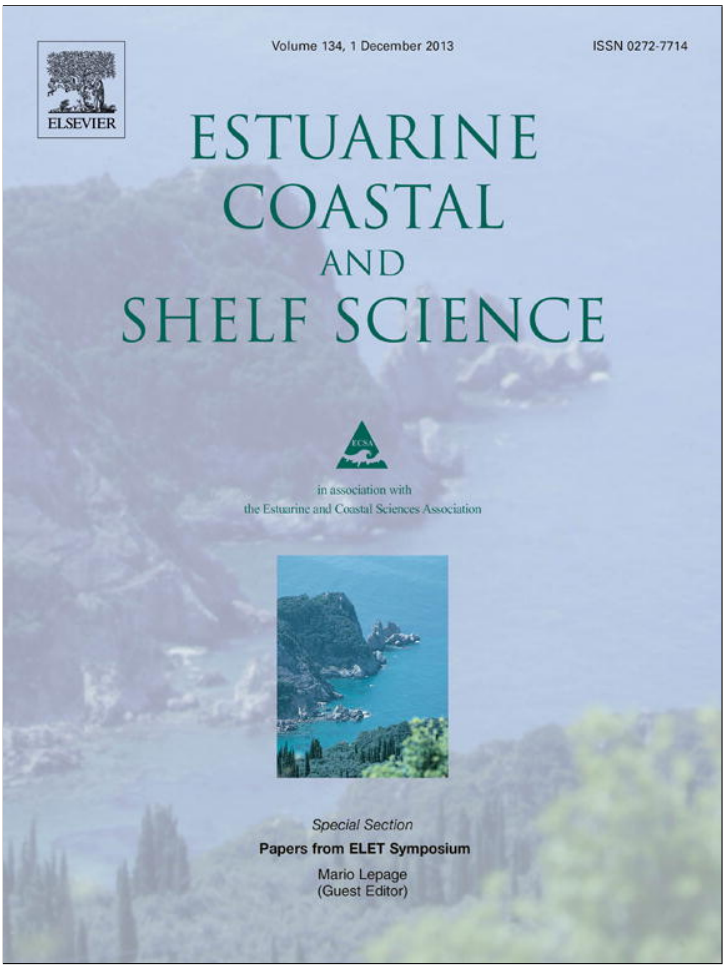

Estuarine, Coastal and Shelf Science 134 (2013) 88–97

Contents lists available at ScienceDirect

Estuarine, Coastal and Shelf Science

journal homepage: www.elsevier.com/locate/ecss

Object-based benthic habitat mapping in the Florida Keys from hyperspectral imagery

Caiyun Zhang [a,*], Donna Selch [a], Zhixiao Xie [a], Charles Roberts [a], Hannah Cooper [a], Ge Chen [b]

[a] Department of Geosciences, Florida Atlantic University, Boca Raton, FL 33431, USA
[b] Department of Marine Technology, Ocean University of China, Qingdao 266100, China

ARTICLE INFO

Article history:
Received 20 May 2013
Accepted 27 September 2013
Available online 7 October 2013

Keywords:
hyperspectral remote sensing
benthic habitat classification
OBIA
machine learning
Florida Keys

ABSTRACT

Accurate mapping of benthic habitats in the Florida Keys is essential in developing effective management strategies for this unique coastal ecosystem. In this study, we evaluated the applicability of hyperspectral imagery collected from Airborne Visible/Infrared Imaging Spectrometer (AVIRIS) for benthic habitat mapping in the Florida Keys. An overall accuracy of 84.3% and 86.7% was achieved respectively for a group-level (3-class) and code-level (12-class) classification by integrating object-based image analysis (OBIA), hyperspectral image processing methods, and machine learning algorithms. Accurate and informative object-based benthic habitat maps were produced. Three commonly used image correction procedures (atmospheric, sun-glint, and water-column corrections) were proved unnecessary for small area mapping in the Florida Keys. Inclusion of bathymetry data in the mapping procedure did not increase the classification accuracy. This study indicates that hyperspectral systems are promising in accurate benthic habitat mapping at a fine detail level.

1. Introduction

1.1. Importance of coral reefs and benthic habitat mapping

Coral reef ecosystems worldwide are in crisis due to anthropogenic activities (e.g., fishing, mining, and pollution) and global climate change (e.g., ocean warming) (Baker et al., 2008). As the "rain forests of the sea", coral reefs are the most diverse ecosystem with a variety of marine species and millions of undiscovered organisms. Their rich biodiversity is considered a living museum and key to finding new medicines in the 21st century. Reefs also offer valuable socio-economic resources to human societies worth billions of dollars each year (NOAA, 2000). Benthic habitats are places on or near the sea floor where aquatic organisms live. These beds of seagrass, coral reef, areas of mud, and sand provide shelter to a rich array of animals. There is a growing need to map benthic habitats of the reef environment in order to provide rapid assessment of health and stress response of these vulnerable ecosystems.

The Florida Keys are the third largest barrier reef ecosystem in the world. They are not only threatened by global climate change and human activities, but also frequently damaged by hurricanes and tropical storms (Rohmann and Monaco, 2005). A range of research projects have been conducted for the conservation and management of the Florida Keys (Florida Keys National Marine Sanctuary, 2013), many of which need the benthic habitat information of this area. Precise mapping of benthic habitats in the Florida Keys is critical for developing management strategies that balance the protection of these habitats with their use (Rohmann and Monaco, 2005).

1.2. Application of remote sensing in benthic habitat mapping

Previous mapping efforts of benthic habitats in the Florida Keys have focused on the visual interpretation of aerial photographs, leading to a map product released in 1998 (Benthic Habitats of the Florida Keys, 2013). Updating this product is difficult because the manual interpretation procedure is labor-intensive and time-consuming.

Researchers have applied remote sensing data for automated benthic habitat mapping in shallow coastal waters (i.e. <20 m water depth) (Mumby et al., 2004; Andréfouët, 2008). Such research can be grouped into three categories. The first is the application of multispectral sensors with a coarse spatial resolution (i.e. 20–30 m or larger), such as Landsat data (e.g., Purkis and Pasterkamp, 2004). This type of data may have limited effectiveness in mapping heterogeneous benthos due to its relatively coarse spatial resolution. In addition, multispectral data are unable to

* Corresponding author.
E-mail address: czhang3@fau.edu (C. Zhang).

0272-7714/$ – see front matter © 2013 Elsevier Ltd. All rights reserved.
http://dx.doi.org/10.1016/j.ecss.2013.09.018

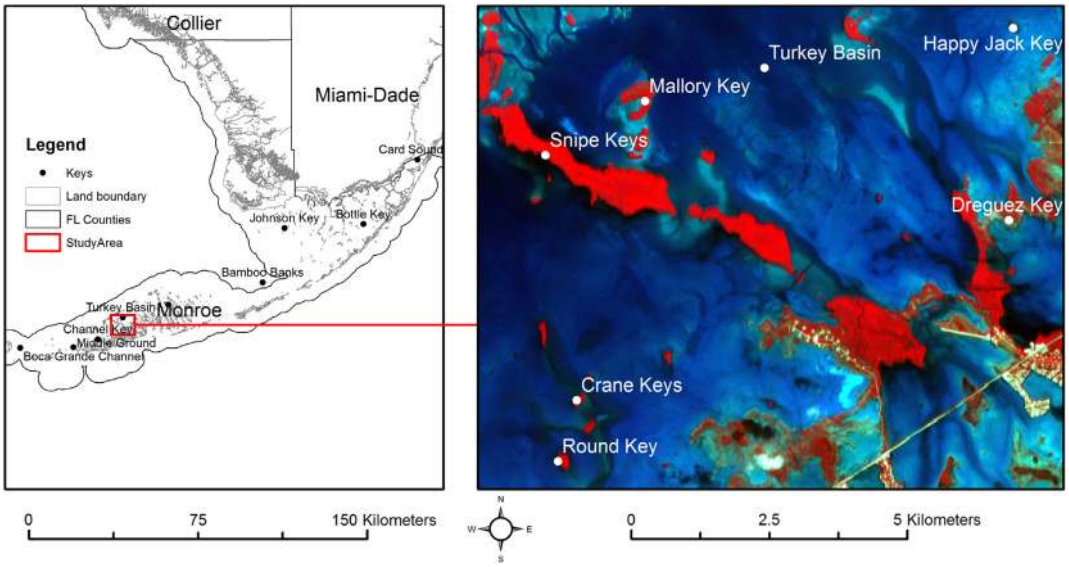

Fig. 1. Map of the Florida Keys and study area shown as a false color composite generated from AVIRIS hyperspectral data.

discriminate more than seven different habitat classes because of their poor spectral resolution (Benfield et al., 2007). The second is the employment of multispectral data with a fine spatial resolution (i.e. 4 m or smaller), such as imagery collected from IKONOS and QuickBird (e.g., Maeder et al., 2002; Mumby and Edwards, 2002; Andréfouët et al., 2003; Mishra et al., 2006; Phinn et al., 2012; Zapata-Ramírez et al., 2013). This type of data is able to produce higher accuracies than Landsat data for regions with low to intermediate numbers of habitat classes, but again cannot be used reliably for mapping fine descriptive detail (e.g., more than 10 classes) (Mumby and Edwards, 2002). The third is the utilization of hyperspectral data, such as imagery collected from Earth Observation-1 (EO-1)/Hyperion, Compact Airborne Spectrographic Imager (CASI), and HyMap (e.g., Mishra et al., 2007; Lesser and Mobley, 2007; Phinn et al., 2008; Bertels et al., 2008; Fearns et al., 2011; Pu et al., 2012; Botha et al., 2013). Studies have illustrated that this type of data yields higher accuracies than multispectral data in mapping areas with low to intermediate numbers of habitats, but evaluation of their potential in mapping fine descriptive habitats is limited (Lesser and Mobley, 2007).

1.3. Mapping methods

Most researchers conduct the pixel-based classification in mapping benthos. This may lead to a “salt-and pepper” effect if the mapping area has a diversity of habitats with a high spatial heterogeneity. Object-Based Image Analysis (OBIA) can remove this effect. These techniques first decompose an image scene into relatively homogeneous objects or areas and then classify these areas instead of pixels. OBIA has been well developed and applied in terrestrial studies in the past decade, as evidenced by a review paper from Blaschke (2010). However, such methods have not been utilized sufficiently in benthic habitat mapping. Benfield et al. (2007) compared the object- and pixel-based methods in mapping coral reefs and associated sublittoral habitats in Pacific Panama using multispectral imagery. They found that object-based classifications can produce more accurate results than pixel-based approaches. Phinn et al. (2012) applied the OBIA techniques for mapping geomorphic and ecological zones on coral reefs from QuickBird data. They found that OBIA is effective to explicitly map regional scale benthic community composition from fine spatial resolution satellite imagery.

1.4. Classification algorithms in benthic habitat mapping

Image classification is a crucial stage in remote sensing image analysis and the selection of classifiers may largely impact the final result (Benfield et al., 2007). Previous benthic habitat mapping studies commonly applied the traditional image classifiers such as Maximum Likelihood (ML) (e.g., Mumby and Edwards, 2002; Andréfouët et al., 2003; Benfield et al., 2007; Pu et al., 2012; Zapata-Ramírez et al., 2013). The ML method requires the spectral response of each class to follow a Gaussian distribution, which is not guaranteed for hyperspectral data. Contemporary machine learning techniques have received little attention in benthic habitat mapping, although they can produce higher accuracies than ML classifier especially in classifying hyperspectral data (Zhang and Xie, 2012, 2013a,b). There is a need to expand machine leaning techniques into benthic habitat mapping as an alternative to ML algorithm.

1.5. Objectives

For this study, we explored the performance of a machine learning algorithm, Random Forest (RF), for object-based benthic habitat mapping at two levels (group- and code- level) in the Florida Keys using hyperspectral imagery. Most previous studies applied traditional classifiers and mapped the benthos at the pixel level. Few studies mapped benthic habitats through a combination of OBIA, machine learning classifiers, and hyperspectral image analysis. Moreover, few researchers examined the applicability of hyperspectral sensors in mapping a larger number of benthos (e.g. more than 10 types) to investigate their potential for fine descriptive habitat mapping. To this end, the main objective of this study is to effectively integrate OBIA, machine learning techniques, and hyperspectral analysis into the automated benthic habitat mapping procedure; and secondarily to explore the capability of hyperspectral systems in habitat mapping at a coarse detail level (3-class, group-level) and a fine detail level (12-class, code-level).

Researchers most commonly conducted three image calibration procedures known as atmospheric correction, sun-glint correction, and water-column correction in benthic habitat mapping. Detailed descriptions of these three corrections are presented in Section 2.4. Few studies systematically evaluated the

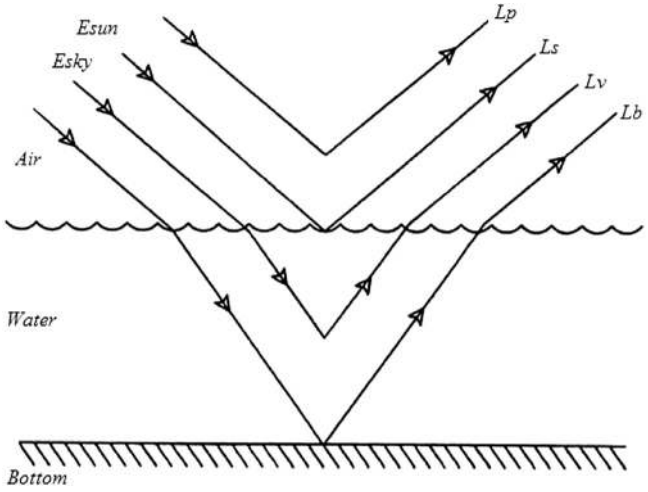

Fig. 2. The energy–matter interactions over a water body (after Bukata et al., 1995).

impacts of these three corrections on the accuracy of classifying benthos. We therefore additionally investigated whether these three corrections are mandatory in benthic habitat mapping over the Florida Keys. Water depth is believed to be an important factor that influences benthic covers in a reef environment (Bertels et al., 2008) and has been frequently included in the manual mapping procedure (e.g., Rohmann and Monaco, 2005; Walker, 2009). However, little work has explored the contribution of bathymetry data to benthic habitat mapping in an automated procedure. Thus we also examined whether the bathymetry data can benefit the benthic habitat mapping using data fusion techniques. It is expected that the bathymetry data can complement the spectral information of optical imagery to improve the benthic habitat classification.

2. Material and methods

2.1. Study area

The study area, with an approximate size of 92 km^2, is located in the lower Florida Keys (Fig. 1). The Florida Keys are a coral cay archipelago beginning at the southeastern tip of the Florida peninsula and extending in a gentle arc south–southwest and then westward to the inhabited islands known as Key West. The study site has a tropical climate and its environment is similar to the Caribbean. This area is characterized by spectacular coral reefs, extensive seagrass beds, and mangrove-fringed islands. It is one of the world's most productive ecosystems with more than 6000 species of marine life and 250 species of birds nesting in this region. The substrate consists of hardbottom, continuous seagrass, and patch seagrass for the selected region. The water depth varies from 0 to 3.5 m, a typical shallow water body. Here shallow water is characterized with a water depth less than 20 m to be consistent with the project "Mapping Southern Florida's Shallow-water Coral Ecosystems: An Implementation Plan" directed by National Oceanic and Atmospheric Administration (NOAA) (Rohmann and Monaco, 2005). Note that NOAA's plan still focuses on *in-situ* campaigns and manual interpretation procedure.

2.2. Data

Data sources used in this study include hyperspectral imagery collected by Airborne Visible/Infrared Imaging Spectrometer (AVIRIS), bathymetry data, and benthic habitat reference maps. AVIRIS

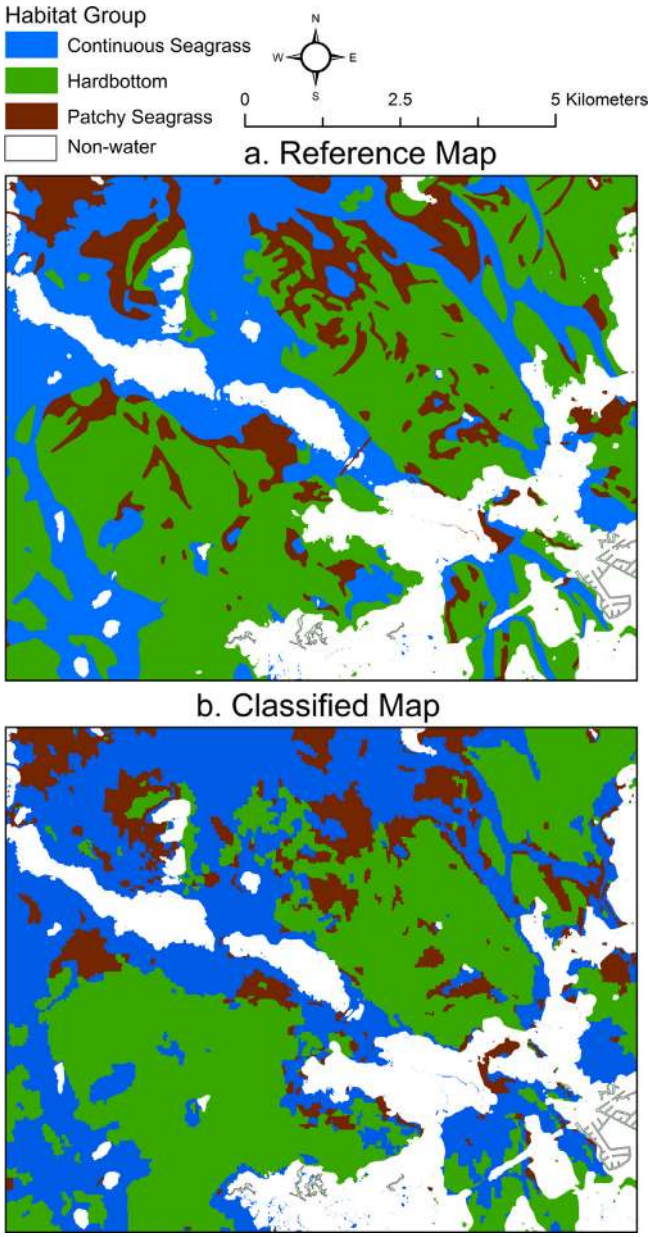

Fig. 3. Group-level benthic habitat maps from (a) reference data and (b) classification result.

collects calibrated hyperspectral data in 224 contiguous spectral channels with wavelengths from 0.4 μm to 2.5 μm. AVIRIS data over the study area were collected on November 19, 1992 with a spatial resolution of 17 m. The bathymetry data are from the National Geophysical Data Center (NGDC) of NOAA. The NGDC produced a Digital Elevation Model (DEM) with a spatial resolution of 1/3 arc-second (~10 m) for the Florida Keys by combining many available elevation data sources (Grothe et al., 2011). The benthic habitat reference data were produced through a seven-year project cooperatively conducted by the National Ocean Service of NOAA and the Florida Fish and Wildlife Research Institute. In this project benthic habitats were visually interpreted from a series of aerial photographs collected between December 1991 and April 1992. Habitats were classified into 4 major categories (referred to as the group-level classes) and 24 subcategories (referred to as the code-level classes) based on a classification scheme developed in the project

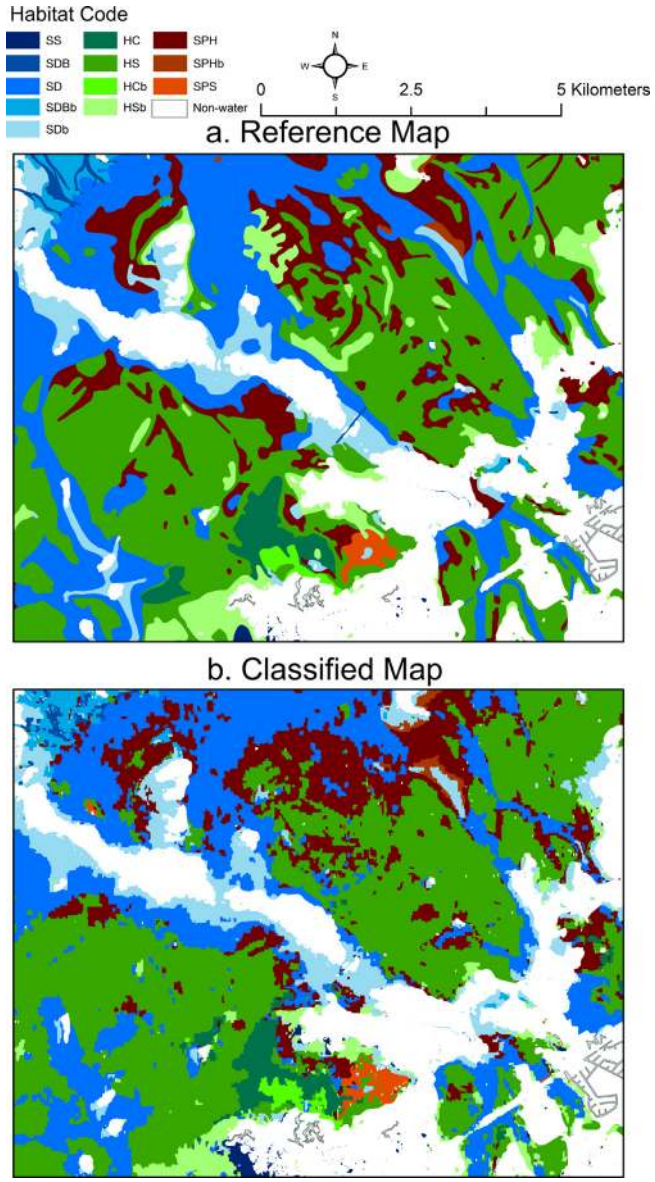

Fig. 4. Code-level benthic habitat maps from (a) reference data and (b) classification result.

(Benthic Habitats of the Florida Keys, 2013). This dataset is currently serving as the baseline in the management of Florida Keys. All these data sources are available in digital format to the public at no cost.

We extracted the group- and code-level reference data for our study site, as shown in Figs. 3a and 4a, respectively. Three group-level communities were found: hardbottom, continuous seagrass, and patchy seagrass. Seven code-level habitats were observed: HC (*soft coral*, *hard coral*, *sponge*, and *algae hardbottom*), HS (*hardbottom with perceptible seagrass (<50%)*), SD (*moderate to dense, continuous beds of seagrass*), SDB (*moderate to dense nearly continuous beds (seagrass>50%), with blowouts and/or sand or mud patches*), SS (*sparse continuous beds of seagrass*), SPH (*dense patches of seagrass (>50%) in a matrix of hardbottom*), and SPS (*dense patches of seagrass in a matrix of sparse seagrass*). The code-level habitats located over the banks have distinctive signatures on the aerial photographs, thus they have been separately labeled, resulting in five extra codes: HCb, HSb, SDb, SDBb, and SPHb (b represents banks). These habitats need to be identified and mapped from the hyperspectral imagery. Descriptions of these habitats are listed in the Appendix Table. We spatially randomly selected 498 group-level and 2254 code-level sample objects respectively from the reference data. The sample collection followed a stratified random sampling strategy in which a fixed percentage of samples are selected for each class. The number of samples for each class was roughly estimated based on the image segmentation results and reference maps. The image segmentation procedure is detailed in Subsection 2.5. The selected sample data at the group-level and code-level were split into two halves with one used for calibration (training) and the other used for validation (testing).

2.3. Data preprocessing

Spectral channels with a low signal-to-noise ratio were dropped from the AVIRIS imagery, leading to 30 visible bands and 86 near-infrared (NIR) and shortwave infrared (SWIR) bands for further analysis. An image to image rectification was employed to georeference the AVIRIS data with the use of the U.S. Geological Survey (USGS)'s Digital Orthophoto Quadrangles (DOQs). Note that the same DOQs were also utilized in the production of the benthic habitat reference data. In this way the hyperspectral imagery was geographically aligned with the reference data. Non-water areas were masked out using the bathymetry data. Hyperspectral data contains a tremendous amount of redundant spectral information. The Minimum Noise Fraction (MNF) method (Green et al., 1988) is commonly used to reduce the high dimensionality and inherent noise of hyperspectral data. We conducted the MNF transformation in ENVI 4.7 and selected the most useful and spatially coherent eigenimages for the classification. To examine the impact of MNF transformation on the classification, the original AVIRIS imagery with 30 visible bands was also classified for comparison purpose.

2.4. Three image corrections

The total radiance, (L_t) recorded by a remote sensor above the water surface is a function of the electromagnetic energy from four sources identified in Fig. 2 (Bukata et al., 1995):

$$L_t = L_p + L_s + L_v + L_b \quad (1)$$

where L_p is the radiance recoded by a sensor from the downwelling solar (E_{sun}) and sky radiation (E_{sky}) that never actually reaches the water surface; and L_s, L_v, and L_b are the radiances from the air–water surface, water column, and bottom respectively.

To map the benthic habitats, the radiance from the bottom (L_b) has been commonly separated or predicted first, which involves three corrections: radiometric correction to remove atmospheric attenuation (L_p), sun-glint correction to remove the specular reflectance from water surface (L_s), and water-column correction to remove the effects of water attenuation (L_v). Many algorithms have been developed for the above three corrections. The most frequently adopted ones, as briefly described below, were examined in this study.

2.4.1. Atmospheric correction

The Fast Line-of-Sight Atmospheric Analysis of Spectral Hypercubes (FLAASH) algorithm is an atmospheric correction module that has been widely used for hyperspectral data calibration. It corrects images for atmospheric water vapor, oxygen, carbon dioxide, methane, ozone, and molecular and aerosol

scattering using a MODTRAN 4 + radiation transfer code solution computed from each image and each pixel in the image (Exelis Visual Information Solutions, Inc., 2009). FLAASH typically consists of three steps in the correction (Matthew et al., 2003): the retrieval of atmospheric parameters, the solution of radiative transfer equation, and the optional post-processing to remove artifacts remaining from the correction process. Evaluation of the FLAASH algorithm for AVIRIS data illustrates that this algorithm is capable of generating accurate surface reflectance spectra from hyperspectral imagery, at least under conditions of clear to moderate aerosol/haze, low to moderate water vapor, and nadir viewing from any altitude between the ground and the top of the atmosphere (Matthew et al., 2003). For this study, we applied the FLAASH algorithm in ENVI to calibrate the hyperspectral imagery. The detailed implementation of FLAASH for AVIRIS data can be found in the manual of the Exelis Visual Information Solutions (2009).

2.4.2. Sun glint correction

Sun glint is a serious confounding factor for remote sensing of water column properties and benthos. A range of sun-glint correction models was proposed, as reviewed by Kay et al. (2009). For shallow waters researchers commonly use the method developed by Hedley et al. (2005) for sun-glint correction. In this algorithm, regression analysis is performed between NIR and visible bands first using a sample set of pixels to derive a series of regression slopes. The sun-glint corrected pixel brightness value is then calculated using the equation $R' = R_i - b_i \times (R_{NIR} - MIN_{NIR})$, where R' is the corrected brightness values; R_i and R_{NIR} are the original pixel visible and NIR brightness values respectively; MIN_{NIR} is the ambient NIR level which is the minimum NIR brightness value in the selected samples; and b_i is the regressed slope between visible band i and NIR band. There are two assumptions in this algorithm: the brightness in the NIR is composed only of sun glint and a spatially constant "ambient" NIR component, and the amount of sun glint in the visible bands is linearly related to the brightness in the NIR band. For this study, we derived the R_{NIR} using the average of the brightness values covering NIR and SWIR in the AVIRIS data, which should be more robust than that of using one selected NIR channel. Similarly, the average value was used in the regression analysis to produce the regression slopes b_i.

Kutser et al. (2009) developed a sun glint correction method to process hyperspectral imagery. There are two assumptions in their method: 1) there is no spectral feature in a remote sensing reflectance spectrum at 760 nm; and 2) the depth of the oxygen absorption feature at 760 nm is proportional to the amount of glint in this pixel. The depth of absorption feature is calculated by $D = [R(739) + R(860)]/2 - R(760)$, where D is the depth of oxygen absorption and $R(739)$, $R(760)$, and $R(860)$ are reflectances at these particular wavelengths. D is then normalized by taking all negative D values equal to zero and dividing the results with the maximum D value. The new water reflectance R_w is then calculated by $R_w = R - G(\lambda) \times D_{norm}(x, y)$, where R is the unglinted image, $G(\lambda)$ is the glint spectrum and $D_{norm}(x, y)$ is the normalized D image. We tested the algorithms developed by Hedley et al. (2005) and Kutser et al. (2009) respectively.

2.4.3. Water-column correction

Water-column correction, a process to remove the influence of water depth on bottom reflectance, is also one of the most commonly cited difficulties for remote sensing of benthos. Theoretically developed analytical models usually require many parameters such as absorption and backscattering coefficients for each channel in order to effectively simulate the attenuation of water. Application of these analytical models is very challenging for hyperspectral data since there are more parameters to be specified. Thus, an image-based approach developed by Lyzenga (1981) is often used to compensate for the effect of variable depth when mapping benthos for clear water (e.g., Mumby et al., 1998; Mumby and Edwards, 2002; Andréfouët et al., 2003; Benfield et al., 2007; Pu et al., 2012). Rather than directly predicting the radiance from the bottom, this method calculates a depth invariant bottom index B_{ij} from each pair of visible bands i and j by:

$$B_{ij} = \ln(L_i) - K_i/K_j \times \ln(L_j) \quad (2)$$

where L_i and L_j are the radiance of band i and band j respectively; K_i/K_j is the ratio of water attenuation coefficients of bands i and j, and it is determined from a bi-plot transformed radiance in the two bands L_i and L_j using samples selected from a bottom of uniform substratum but at variable depths. The model assumes that light attenuation follows an exponential decay curve with increasing depth. Two visible bands produce one index. Thus for our case, 30 visible bands can produce 435 indices by permutation. Based on Hamylton (2011), for optimal performance of water-column correction using this method, bands selected for the index calculation must be at least 90 nm apart. This will lead to 30 indices from our hyperspectral data if bands are at a distance of around 100 nm. We tested one image with 435 indices and the other image with 30 derived indices.

2.5. Hierarchical image segmentation

We applied the hierarchical segmentation to generate image objects for two habitat levels. Hierarchical segmentation is defined as a set of segmentations of the same image at different levels of spatial resolution in which coarser levels can be produced by merging regions at finer levels (Beaulieu and Goldberg, 1989). We produced image objects using the Multiresolution Segmentation algorithm in eCognition Developer 8.64.1 (Trimble, 2011). The algorithm starts with single pixel image segments, and merges neighboring segments until a heterogeneity threshold is reached (Benz et al., 2004). The heterogeneity threshold is determined by a user-defined scale parameter, as well as color/shape and smoothness/compactness weights. Image segmentation is scale-dependent and the quality of segmentation and overall object-based classification are heavily dependent on the scale. In order to find the optimal scale for image segmentation we used an unsupervised image segmentation evaluation approach (Johnson and Xie, 2011). This approach conducts a series of segmentations using different scale parameters to identify the optimal scale using an unsupervised evaluation method that takes into account global intra-segment and inter-segment heterogeneity measures. A global score combining a normalized weighted variance and Moran's I value was used to determine the optimal scale for the segmentation. We thus carried out a series of segmentations with the scale parameter ranging from 2 to 20, at an interval of 2. A scale parameter of 12 was found to be optimal for the group-level segmentation. The weights of the MNF layers were set based on their eigenvalues. Equal weights were set for the original imagery in the segmentation. Note that only 30 visible bands were used in the classification because of strong water absorption over the NIR and SWIR region. Color and shape weights were set to 0.9 and 1.0 so that spectral information would be considered more heavily for segmentation. Smoothness and compactness weights were set to

0.5 and 0.5 so as to not favor either compact or non-compact segments.

Code-level image objects were produced using a finer scale based on the result of group-level segmentation. A heuristic method was used to find the optimal scale for the code-level segmentation (Zhang and Xie, 2013b). We randomly selected 10% of the group-level segments and handled each segment as an individual image. We then conducted a series of multiresolution segmentations using six different scale parameters (1–6 at an interval of 1) for each selected segment. Global scores were calculated and the optimal scale was determined as the one with the highest frequency to generate the lowest global score among these selected segments. For this case, a scale parameter of 3 was found to be the optimal scale for code-level segmentation. The other parameters were the same as those used for the group-level segmentation.

2.6. Classification

For this study, we examined a machine learning algorithm Random Forest (RF) for benthic habitat classification. RF is a decision tree based ensemble classifier. Decision trees split the training samples into smaller subdivisions at "nodes" based on decision rules. For each node, tests are performed on the training data to find the most useful variables and variable values for the split. The RF consists of a combination of decision trees where each decision tree contributes a single vote for assigning the most frequent class to an input vector. RF increases the diversity of decision trees by changing the training set using the bagging aggregating method (Breiman, 2001). Bagging creates training data by randomly resampling the original dataset with replacement. A key feature of RF is that the computational complexity is simplified by reducing the number of input features at each node. Different algorithms can be used to generate the decision trees. The RF often adopts the Gini Index (Breiman, 2001) to measure the best split selection. A more detailed description of RF can be found in Breiman (2001) or in a remote sensing context in Chan and Paelinckx (2008). We implemented the RF algorithm using Weka 3.7, an open-source data mining program (Hall et al., 2009). Two parameters must be defined in this method: the number of decision trees to create (k) and the number of randomly selected variables (m) considered for splitting each node in a tree. The computational complexity of the algorithm can be reduced by selecting a smaller m, and k is often set based on trial and error. For our dataset, m was set to 10 and 3 for original data and MNF transformed data respectively. Trials using different number of trees (50–500 at an interval of 50) revealed that $k = 150$ produced the highest accuracy.

2.7. Accuracy assessment

We produced the accuracies of the object-based habitat maps by constructing an error matrix and calculating the Kappa statistics (Congalton and Mead, 1983). Overall accuracy or total accuracy is defined as the ratio of the number of validation samples that are classified correctly to the total number of validation samples irrespective of the class. The Kappa value describes the proportion of correctly classified validation samples after random agreement is removed. We used the nonparametric McNemar test (Foody, 2004) to evaluate the statistical significance of differences in accuracy between different classifications. The difference in accuracy between a pair of classifications is viewed as being statistically significant at a confidence of 95% if the calculated z-score in McNemar test is larger than 1.96.

Table 1
Classification results from different experiments.

Experiment#	Total accuracy (%)	Kappa value	Kappa test (z-score)	McNemar test (z-score)
Group-level classification				
1	75.1	0.61	8.1*	NA
2	84.3	0.76	21.4*	2.8* (1/2)
3	86.3	0.78	22.1*	1.2 (2/3)
4	83.9	0.75	21.1*	0.1.(2/4)
5	78.7	0.67	16.6*	1.8 (2/5)
6	85.5	0.77	22.6*	1.1 (2/6)
7	69.5	0.53	12.1*	4.6*(2/7)
Code-level classification				
1	80.8	0.77	54.5*	NA
2	86.7	0.84	69.2*	4.2* (1/2)
3	87.9	0.85	72.9*	0.5 (2/3)
4	86.9	0.84	69.5*	0.1 (2/4)
5	85.9	0.83	66.3*	0.6 (2/5)
6	87.4	0.85	71.5*	1.5 (2/6)
7	60.1	0.53	30.9*	14.3* (2/7)

Experiment 1 used original imagery with 30 visible bands.
Experiment 2 used MNF transformed imagery.
Experiment 3 used atmospherically corrected imagery.
Experiment 4 used sun-glint corrected imagery.
Experiment 5 used water-column corrected imagery.
Experiment 6 used a fused dataset from MNF transformed imagery and bathymetry data.
Experiment 7 used the Maximum Likelihood classifier.
Experiments 1–6 used the Random Forest classifier.
For the McNemar test, 1/2, 2/3…2/7 refers to the significant test between experiments 1 and 2, 2 and 3…2 and 7.
* Significant at 95% confidence.

3. Results and discussion

3.1. Impact of MNF transformation on the classification

We classified both original data (i.e. 30 visible bands) and MNF transformed data (i.e. 10 MNF layers) to examine the impact of MNF transformation on benthic habitat classifications. The results are displayed in Table 1 with experiments 1 and 2 representing the application of original and MNF transformed data, respectively. The original data generated a lower accuracy. MNF transformation increased the accuracy from 71.5% with a Kappa value of 0.61 to 84.3% with a Kappa value of 0.76 for the group-level classification. To examine the significance of the result, the Kappa z-score statistical test based on the error matrix was conducted. The Kappa z-score values for experiments 1 and 2 are 8.1 and 21.4 respectively (Table 1), which suggests both experiments are significantly better than a random classification at the 95% statistical confidence level. Similarly, for the code-level classification the MNF technique improved the accuracy from 80.8% with a Kappa value of 0.77 to 86.7% with a Kappa value of 0.84. Again, Kappa tests showed that these two classifications are significantly better than random classifications. McNemar tests for both group- and code-level classification illustrated that the improvements from MNF transformed data are statistically significant.

In benthic habitat mapping studies using hyperspectral data, some researchers applied the MNF transformation before classification (e.g., Mishra et al., 2007; Bertels et al., 2008), while others worked directly from the non-transformed data (e.g., Phinn et al., 2008; Pu et al., 2012). Few studies have investigated the impact of MNF transformation on the classification. Our study illustrates that the MNF transformation can significantly improve classification accuracy of the non-MNF transformed data by removing the inherent noise in hyperspectral data. This indicates that the MNF transformation is necessary to

effectively apply the hyperspectral data for benthic habitat mapping.

3.2. Impact of atmospheric correction on the classification

To examine the impact of atmospheric correction on the final classification, we applied the FLAASH module first to the original imagery and then conducted the MNF transformation on the corrected imagery. The classification results from the MNF transformed data are also shown in Table 1 as experiment 3. Compared with experiment 2, the total accuracies and Kappa values increased for both group- and code-level classifications, but McNemar tests show that these improvements are not statistically significant. This suggests the atmospheric correction is not essential for this study area.

Atmospheric correction is not always necessary for certain types of classifications, especially in the terrestrial studies. But for benthic habitat remote sensing, this procedure is generally believed mandatory. For example, Mishra et al. (2007) and Pu et al. (2012) also applied FLAASH atmospheric correction in their hyperspectral benthic habitat mapping studies. Again, few studies have examined whether this correction can impact the classification. Our study demonstrates that it is possible to ignore the atmospheric effects for remote sensing of benthos if the data are not extended through space and/or time for cross-calibration purpose. Most atmospheric correction models assume the distribution of the atmosphere in the entire scene is homogeneous. This indicates that the primary effect from the atmospheric correction will be a simple bias adjustment applied to each band, which has little effect in the final classification accuracy.

3.3. Impact of sun-glint correction on the classification

We applied the sun-glint correction method developed by Hedley et al. (2005) to our data, and then similarly transformed the data using MNF technique to remove the inherent noise. The classification result is shown in Table 1 as experiment 4. The overall accuracy is 83.9% with a Kappa value of 0.75 and 86.9% with a Kappa value of 0.84 for group- and code-level classifications respectively. Kappa statistical tests show that they are significantly better than random classifications, but again, McNemar tests illustrate that there is no significant difference between experiments 2 and 4. We also applied the sun-glint correction algorithm developed by Kutser et al. (2009). The results also show no significant difference between before and after sun-glint corrected data.

Previous studies either applied sun-glint correction or ignored this procedure in multispectral and hyperspectral benthic habitat mapping. No attempts have been made to examine whether the sun-glint correction can impact the final classification. Our study suggests that it is feasible to ignore this procedure when the object-based classification is carried out. Sun glint over an image usually displays a wave like pattern with alternative dark and bright pixels. Directly conducting a pixel-based classification for the uncorrected imagery may strongly impact the accuracy. Conversely, the object-based classification adopts the mean spectral and/or spatial information of a segmented object, which can effectively "smooth" the glint effect over the segmented region, leading to a relatively homogeneous glint across the entire scene. In this way the impact of sun-glint effects can be reduced. In addition, here the hyperspectral imagery has a relative coarse spatial resolution (17 m), which can help smooth out small scale glint effects over the coastal areas, therefore correction is unnecessary. For fine spatial resolution imagery such as IKONOS with severe sun-glint contamination, further tests are needed to investigate the benefit of object-based classification in the procedure.

3.4. Impact of water-column correction on the classification

Similarly, we applied the MNF transformation to the water-column corrected imagery, i.e. the depth invariant bottom index data (495 layers), and selected the useful MNF layers for classification. The results are displayed in Table 1 as experiment 5. A lower accuracy was obtained and no significant difference was revealed between experiments 5 and 2. We also examined the corrected imagery with 30 depth invariant indices which were produced by setting the selected bands 100 nm apart. The classification results are similar to experiment 5 (not shown here).

A few studies have shown that the classification accuracy of coral reefs can be increased significantly after water-column correction by using the same water depth invariant index strategy (Mumby et al., 1998; Nurlidiasari and Budhiman, 2005), while a majority of studies ignored this procedure or simply applied the correction without checking its impact on the final classification. Our results show that this depth correction for accounting for light attenuation did not improve the classification accuracy. The algorithm adopted in this study for water-column correction requires the same bottom type occur over a wide range of depth, which is poorly suited for the shallow waters in the Florida Keys. For mapping small areas with low bathymetric variability, this correction procedure can be ignored. Also note that for implementation of this algorithm, it relies on subtracting a deep-water value from each pixel regardless of substrate type. This is difficult to implement if the deepest region is only several meters.

3.5. Contribution of bathymetry data to benthic habitat mapping

We combined the MNF transformed imagery and bathymetry data using a pixel level fusion strategy and then conducted an object-based classification. The results are shown as experiment 6 in Table 1. A total accuracy of 85.5% with a Kappa value of 0.77 was obtained for the group-level classification; and for the code-level classification, a total accuracy of 87.4% with a Kappa value of 0.85 was produced. Again, we carried out the Kappa statistical tests and McNemar tests for the classifications. The results illustrated that they are significantly better than a random classification, but not significantly different from experiment 2 which used the MNF transformed data alone. This confirms that depth compensation in the classification procedure is unnecessary. A variety of terrestrial studies have demonstrated that the elevation information is useful in land cover mapping (Lu and Weng, 2007), but in an aquatic environment, no benefits of bathymetry information have been revealed in benthic habitat classification, at least in our study area.

3.6. Comparison of Maximum Likelihood and Random Forest classifiers

Selection of classifiers is an important factor in the classification. For comparison purpose, we applied the commonly used Maximum Likelihood (ML) classifier to the MNF transformed imagery and the object-based classification results are shown as experiment 7 in Table 1. The ML method presented a poor result with a total accuracy of 69.5% and Kappa value of 0.53 for the group-level classification. For the code-level classification, the total accuracy is 60.1% with a Kappa value of 0.53. Random Forest achieved a significantly better result than ML classifier with a *z*-

Table 2
Error matrix for the group-level classification.

Group#	1	2	3	Row total	PA (%)
1	79	4	9	92	86.0
2	4	99	2	105	94.3
3	10	10	36	56	64.3
Col. total	93	113	47	Total accuracy: 84.3%	
UA (%)	84.9	87.6	76.6	Kappa value: 0.76	

UA: User's Accuracy; PA: Producer's Accuracy.
Classification result is displayed in row, and the reference data is displayed in column.
Groups 1–3 represent for continuous seagrass, hardbottom, and patchy seagrass respectively.

score value of 4.6 and 14.3 for group- and code- level classifications respectively from the McNemar tests (Table 1). Both classifiers produced significantly better results than a random classification (Table 1). ML classifier may yield an accurate classification result if the feature of habitats in the dataset is normally distributed. But if the data are anomalously distributed, non-parametric classifiers may demonstrate a better classification result (Lu and Weng, 2007). Hyperspectral data and their corresponding transformed imagery usually do not follow a normal distribution, thus a non-parametric algorithm is desirable. Our study reveals that the Random Forest method had a good performance for habitat classification. Other contemporary machine learning classifiers such as Support Vector Machines (SVMs) and neural networks also have good performances in classifying hyperspectral imagery (Zhang and Xie, 2012, 2013a,b). Combining the outcomes from this type of classifier using a decision fusion procedure (known as classifier ensemble techniques in remote sensing) may have potential to improve the classification accuracy (Zhang and Xie, 2013a). This should be examined in the future.

3.7. Object-based benthic habitat mapping

According to Fleiss (1981), Kappa values larger than 0.75 suggest strong agreement. Landis and Koch (1977) suggest that Kappa values larger than 0.81 indicate an almost perfect agreement. By using the MNF transformed data and Random Forest classifier, a Kappa value of 0.76 and 0.84 have been achieved for group- and code-level classification respectively in experiment 2. This indicates that benthic habitats can be effectively mapped by combining OBIA, hyperspectral systems, and machine learning techniques. Object-based benthic habitat maps were thus produced for two levels, as shown in Figs. 3b and 4b. The object-based habitat map is more informative and useful than a traditional pixel-based one that may be noisy if the study area has a high degree of spatial and spectral heterogeneity. For comparison, the group- and code-level reference maps are shown in Figs. 3a and 4a respectively. There is a general agreement on the spatial distribution of habitat types between the reference and classification maps, with most regions occupied by continuous seagrass and hardbottom communities. Further examination revealed that some small patches and strips were misclassified in the classified maps, which is mainly caused by the relatively poor spatial resolution of the hyperspectral data (17 m). Application of fine spatial resolution hyperspectral data may solve this problem, but data collection is costly. A recent work from Zhang (2013) examined the potential of data fusion techniques to solve this problem for benthic habitat mapping. In Zhang (2013)'s study, the fine spatial resolution aerial photography is segmented first to generate image objects and extract object features (i.e. textures). The extracted features are then combined with pixel-level values of hyperspectral data to generate a fused dataset. The fused dataset produced a higher accuracy than using each individual data alone. Small patches and linear/narrow features were well mapped due to the fine spatial resolution aerial photography. Thus data fusion techniques can be used as an alternative to reduce the misclassification of small patches and strips in the benthic habitat mapping.

The generated error matrixes for two classified maps are listed in Tables 2 and 3. For the group-level classification, the producer's accuracies varied from 64.3% to 94.3% and the user's accuracies varied from 76.6% to 87.6%. For the code-level classification, the producer's accuracy was in the range of 57.1%–95.7%, and the user's accuracy was in the range of 75.9%–100.0%. As expected patchy seagrass and code-level communities present as strips had a relatively lower accuracy. Note that a lower accuracy (84.3%) was obtained for the simple classification (group-level, 3-class) and a higher accuracy (86.7%) was produced for the complex classification (code-level, 12-class). This is different from the results reported in previous studies which found a trend of decreasing accuracy with increasing habitat complexity (e.g., Andréfouët et al., 2003; Pu et al., 2012). As discussed in the Introduction, application of multispectral data may have problems in complex classifications due to their poor spectral resolution; but for the application of hyperspectral data in benthic habitat mapping, the accuracy may largely depend on the degree of complexity of the representative

Table 3
Error matrix for the code-level classification.

Code	HC	HCb	HS	HSb	SD	SDB	SDBb	SDb	SPH	SPHb	SPS	SS	Row total	PA (%)
HC	24	1	5	1					1				32	75.0
HCb		12						1				1	14	85.7
HS	1		313	2	4			1	6				327	95.7
HSb	2	1	11	70				4			1	4	93	75.3
SD			8		198			3	6				215	92.1
SDB			1			16	5	6					28	57.1
SDBb			1			2	40	4	1				48	83.3
SDb				4	5	1		101	1		1		113	89.4
SPH			12	2	15			4	140				173	80.9
SPHb					1			3		6			10	60.0
SPS	1				1			4			16	2	24	66.7
SS			2	3	2			2				41	50	82.0
Col. Total	28	14	353	82	226	19	45	133	155	6	18	48	Total accuracy: 86.7%	
UA (%)	85.7	85.7	88.7	85.4	87.6	84.2	88.9	75.9	90.3	100.0	88.9	85.4	Kappa value: 0.84	

UA: User's accuracy; PA: Producer's accuracy.
Classification result is displayed in row, and the reference data is displayed in column.

spectral signature for each class. For a simple level classification with a small number of classes, each class has several sub-categories, leading to multiple spectral signatures across the scene. Thus the training samples for each class are more heterogeneous, which will add spectral variation within a class and spectral confusion between classes. Consequently, a lower accuracy can occur. In contrast for a more detailed level classification, each individual class can have relatively homogeneous training samples which will result in higher classification accuracy. This indicates that hyperspectral systems are not only able to map a fine level of benthic habitats, but also promising to achieve higher classification accuracy than a coarse level mapping.

4. Conclusions

For this study we evaluated the applicability of AVIRIS hyperspectral imagery with an intermediate spatial resolution (i.e. 17 m) for benthic habitat mapping in the Florida Keys. We combined the object-based image analysis (OBIA), hyperspectral image processing methods, and machine learning techniques in the mapping procedure. We also examined the impacts of three image corrections on the classification accuracy.

Our study reveals that hyperspectral data are promising for automated benthic habitat mapping in the Florida Keys. Accurate and informative habitat maps were produced. A total accuracy of 84.3% was obtained for the group-level classification, and a total accuracy of 86.7% was achieved for a code-level classification with 12 code communities. Hyperspectral systems have the capability to produce higher classification accuracy in discriminating fine descriptive benthos than coarse level mapping. However, hyperspectral data with a relatively coarse spatial resolution are problematic to mapping small patches and linear/narrow features, which can be mitigated by combining fine spatial resolution multispectral data with hyperspectral data using data fusion techniques.

Minimum Noise Fraction (MNF) data transformation is an important step in benthic habitat mapping when hyperspectral data are applied. This preprocess removes the inherent noise in the hyperspectral data, improves the classification accuracy, and reduces the data dimensionality to decrease the computational cost. Three commonly used image processing procedures in benthic habitat mapping (atmospheric correction, sun-glint correction, and water-column correction) had no impacts on the classification accuracy. These three calibrations are unnecessary, at least for small area mapping. Bathymetry data have not shown contribution to the classification accuracy in this study.

Benthic habitat mapping is important in the conservation and management of the world's coral reef ecosystems. It provides an inventory of habitat types and their statistics, and the location of environmentally sensitive areas, as well as the hot spots of habitat diversity. An accurate and informative map can guide the managers to effectively plan the networks of protected areas and monitor the degree of habitat fragmentation. An integration of hyperspectral systems, OBIA, and machine learning techniques had a good performance for habitat mapping in the Florida Keys. Considerable additional work is needed to investigate whether such procedures are useful in other coral reefs with different assemblages of benthos. With the increasing availability of hyperspectral data, it is anticipated that this study will stimulate further hyperspectral remote sensing research and applications in many other marine ecosystems of the world.

Acknowledgements

Dr. Ge Chen appreciates the support from the Natural Science Foundation of China under Project 613111035.

Appendix Table

Descriptions of the habitats found in the selected study area (from Benthic Habitats of the Florida Keys, http://flkeysbenthicmaps.noaa.gov/).

Groups	Codes
Hardbottom	*HC: Soft coral, hard coral, sponge, algae.* Benthic community (no perceptible seagrass) is variable and typically a function of sediment, water, depth, and exposure to wind and current. It may also include solitary hard corals, *Porites* sp., *Sideratrea* sp., and *Manicina* sp. Shallowest zones (<1 m) may include only attached or drift algae; soft corals are usually more common in deeper zones. *HS: Hardbottom with perceptible seagrass (<50%).* Usually in patches, seagrasses occur in depressions and basins where adequate sediment has accumulated, but constitute <50% bottom coverage. Hardbottom may include solitary hard corals and soft corals, but most often sponges and benthic algae (attached or in draft).
Continuous seagrass	*SD: Moderate to dense, continuous beds.* Solid, continuous Thalassia, Syringodium, and Halodule, individually or in mixed beds. Widespread in occurrence with range in depth from intertidal (bank) to approximately 10 m. *SDB: Moderate to dense, nearly continuous beds (seagrass>50%), with blowouts and/or sand or mud patches.* Solid, continuous Thalassia or Syringodium, rarely Halodule, individually or in mixed beds. Widespread in occurrence with range in depth from intertidal (bank) to approximately 10 m. Moderate to high energy regimes. Here, blowouts or patches are dispersed as holes in otherwise continuous seagrass beds. Usually found on reef tract and near entrances to tidal channels and passes. A common habitat in back country of middle keys with large water movements between the Gulf of Mexico and Atlantic Ocean. *SS: Sparse, continuous beds.* Areas where seagrasses occur in low density. Typically in shallow protected bays where physical conditions or substrate limits development. It may be hard to distinguish signature on aerial photographs from barren bottom, requiring ground truthing.
Patchy seagrass	*SPH: Dense patches of seagrass (>50%) in a matrix of hardbottom.* One of the most common habitat types; patches occur in areas where a thin sediment layer over flat natural rock precludes development of seagrasses. Often numerous in number, highly visible on aerial photographs *SPS: Dense patches of seagrass in a matrix of sparse seagrass.* Depressional features with deep sediment allow denser development of seagrasses than on surrounding bottoms where only a thin layer may be present. May be difficult to discern on aerial photographs from seagrass patches in hardbottom. May occur more in deeper water or protected bays

Notes: A special modifier "b" is attached to a specific code type to indicate banks when applicable. For example HCb, and SDBb. Description: Intertidal seagrass and some hardbottom communities, even if only intertidal at spring low tides, often open water features or extending out from a shoreline. Distinctive signature on aerial photography is compared to surrounding bottom. Sometimes burned off patches are present on bank top. If these patches become large enough, they are mapped as separate bare areas.

References

Andréfouët, S., 2008. Coral reef habitat mapping using remote sensing: a user vs producer perspective. implications for research, management and capacity building. J. Spat. Sci. 53, 113–129.

Andréfouët, S., Kramer, P., Torres-Pulliza, D., Joyce, K.E., Hochberg, E.J., Garza-Perez, R., Mumby, P.J., Riegl, B., Yamano, H., White, W.H., Zubia, M., Brock, J.C., Phinn, S.R., Naseer, A., Hatcher, B.G., Muller-Karger, F.E., 2003. Multi-sites evaluation of IKONOS data for classification of tropical coral reef environments. Rem. Sens. Environ. 88, 128–143.

Baker, A.C., Glynn, P.W., Riegl, B., 2008. Climate change and coral reef bleaching: an ecological assessment of long-term impacts, recovery trends and future outlook. Estuar. Coast. Shelf Sci. 80, 435–471.

Beaulieu, J.M., Goldberg, M., 1989. Hierarchy in picture segmentation: a stepwise optimal approach. IEEE Trans. Pattern Anal. Mach. Intell. 11, 150–163.

Benfield, S.L., Guzman, H.M., Mair, J.M., Young, J.A.T., 2007. Mapping the distribution of coral reefs and associated sublittoral habitats in Pacific Panama: a comparison of optical satellite sensors and classification methodologies. Int. J. Rem. Sens. 28, 5047–5070.

Benthic Habitats of the Florida Keys, http://flkeysbenthicmaps.noaa.gov/, (accessed on 17.04.13.).

Benz, U., Hofmann, P., Willhauck, G., Lingenfelder, I., Heynen, M., 2004. Multi-resolution, object-oriented fuzzy analysis of remote sensing data for GIS-ready information. ISPRS J. Photogramm. Rem. Sens. 58, 239–258.

Bertels, L., Vanderstraete, T., Coillie, S.V., Knaeps, E., Sterckx, S., Goossens, R., Deronde, B., 2008. Mapping of coral reefs using hyperspectral CASI data; a case study: Fordata, Tanimbar, Indonesia. Int. J. Rem. Sens. 29, 2359–2391.

Blaschke, T., 2010. Object based image analysis for remote sensing. ISPRS J. Photogramm. Rem. Sens. 65, 2–16.

Botha, E.J., Brando, V.E., Anstee, J.M., Dekker, A.G., Sagar, S., 2013. Increased spectral resolution enhances coral detection under varying water conditions. Rem. Sens. Environ. 131, 247–261.

Breiman, L., 2001. Random forests. Mach. Learn. 45, 5–32.

Bukata, R.P., Jerome, J.H., Kondratyev, K.Y., Pozdnyakov, D.V., 1995. Optical Properties and Remote Sensing of Inland and Coastal Waters. CRC, NY, p. 362.

Chan, J.C.-W., Paelinckx, D., 2008. Evaluation of Random Forest and Adaboost tree based ensemble classification and spectral band selection for ecotope mapping using airborne hyperspectral imagery. Rem. Sens. Environ. 112, 2999–3011.

Congalton, R., Mead, R.A., 1983. A quantitative method to test for consistency and correctness in photointerpretation. Photogramm. Eng. Rem. Sens. 49, 69–74.

Exelis Visual Information Solutions, 2009. Atmospheric Correction Module: QUAC and FLAASH User's Guide. Boulder, Colorado, pp. 6–40.

Fearns, P.R.C., Klonowski, W., Babcock, R.C., England, P., Phillips, J., 2011. Shallow water substrate mapping using hyperspectral remote sensing. Cont. Shelf Res. 31, 1249–1259.

Fleiss, J.L., 1981. Statistical Methods for Rates and Proportions, second ed. John Wiley & Sons, New York.

Florida Keys National Marine Sanctuary, http://floridakeys.noaa.gov/, (accessed 17.04.13.).

Foody, G.M., 2004. Thematic map comparison, evaluating the statistical significance of differences in classification accuracy. Photogramm. Eng. Rem. Sens. 70, 627–633.

Green, A.A., Berman, M., Switzer, P., Craig, M.D., 1988. A transformation for ordering multispectral data in terms of image quality with implications for noise removal. IEEE Trans. Geosci. Rem. Sens. 26, 65–74.

Grothe, P.R., Taylor, L.A., Eakins, B.W., Carignan, K.S., Friday, D.Z., Lim, E., Love, M.R., 2011. Digital Elevation Models of Key West, Florida: Procedures, Data Sources and Analysis. NOAA National Geophysical Data Center technical report, Boulder, CO, p. 20.

Hall, M., Frank, E., Holmes, G., Pfahringer, B., Reutmann, P., Witten, I., 2009. The WEKA data mining software, an update. SIGKDD Expl. 11, 1–18.

Hamylton, S., 2011. An evaluation of waveband pairs for water column correction using band ratio methods for seabed mapping in the Seychelles. Int. J. Rem. Sens. 32, 9185–9195.

Hedley, J., Harborne, A., Mumby, P., 2005. Simple and robust removal of sun glint for mapping shallow-water benthos. Int. J. Rem. Sens. 26, 2107–2112.

Johnson, B., Xie, Z., 2011. Unsupervised image segmentation evaluation and refinement using a multi-scale approach. ISPRS J. Photogramm. Rem. Sens. 66, 473–483.

Kay, S., Hedley, J.D., Lavender, S., 2009. Sun glint correction of high and low spatial resolution images of aquatic scenes: a review of methods for visible and near-infrared wavelengths. Rem. Sens. 1, 697–730.

Kutser, T., Vahtmäe, E., Praks, J., 2009. A sun glint correction method for hyperspectral imagery containing areas with non-negligible water leaving NIR signal. Rem. Sens. Environ. 113, 2267–2274.

Landis, J., Koch, G.G., 1977. The measurement of observer agreement for categorical data. Biometics 33, 159–174.

Lesser, M.P., Mobley, C.D., 2007. Bathymetry, water optical properties, and benthic classification of coral reefs using hyperspectral remote sensing imagery. Coral Reef. 26, 819–829.

Lu, D., Weng, Q., 2007. A survey of image classification methods and techniques for improving classification performance. Int. J. Rem. Sens. 28, 823–870.

Lyzenga, D.R., 1981. Remote sensing of bottom reflectance and water attenuation parameters in shallow water using aircraft and Landsat data. Int. J. Rem. Sens. 2, 71–82.

Maeder, J., Narumalani, S., Rundquist, D.C., Perk, R.L., Schalles, J., Hutchins, K., Keck, J., 2002. Classifying and mapping general coral-reef structure using IKONOS data. Photogramm. Eng. Rem. Sens. 68, 1297–1305.

Matthew, M.W., Adler-Golden, S.M., Berk, A., Felde, G., Anderson, G.P., Gorodetzky, D., Paswaters, S., Shippert, M., 2003. Atmospheric correction of spectral imagery: evaluation of the FLAASH algorithm with AVIRIS data. Proc. SPIE 5093, 474–482.

Mishra, D., Narumalani, S., Rundquist, D., Lawson, M., 2006. Benthic habitat mapping in tropical marine environments using QuickBird multispectral data. Photogramm. Eng. Rem. Sens. 72, 1037–1048.

Mishra, D., Narumalani, S., Rundquist, D., Lawson, M., Perk, R., 2007. Enhancing the detection and classification of coral reef and associated benthic habitats: a hyperspectral remote sensing approach. J. Geophys. Res. 112, C08014. http://dx.doi.org/10.1029/2006JC003892.

Mumby, P.J., Clark, C.D., Green, E.P., Edwards, A.J., 1998. Benefits of water column correction and contextual editing for mapping coral reefs. Int. J. Rem. Sens. 19, 203–210.

Mumby, P.J., Edwards, A.J., 2002. Mapping marine environments with IKONOS imagery: enhanced spatial resolution does deliver greater thematic accuracy. Rem. Sens. Environ. 82, 248–257.

Mumby, P.J., Skirving, W., Strong, A.E., Hardy, J.T., Ledrew, E., Hochberg, E.J., Stumpf, R.P., David, L.T., 2004. Remote sensing of coral reefs and their physical environment. Mar. Pollut. Bull. 48, 219–228.

NOAA, March 2000. U.S. Coral Reef Task Force Unveils Groundbreaking Plan to Protect 20 Percent of Reefs by 2010. Earth System Monitor, p. 10.

Nurlidiasari, M., Budhiman, S., 2005. Mapping coral reef habitat with and without water column correction using Quickbird image. Rem. Sens. Earth Sci. 2, 45–56.

Phinn, S., Roelfsema, C., Dekker, A., Brando, V., Anstee, J., 2008. Mapping seagrass species, cover and biomass in shallow waters: an assessment of satellite multispectral and airborne hyper-spectral imaging systems in Moreton Bay (Australia). Rem. Sens. Environ. 112, 3413–3425.

Phinn, S.R., Roelfsema, C.M., Mumby, P.J., 2012. Multi-scale, object-based image analysis for mapping geomorphic and ecological zones on coral reefs. Int. J. Rem. Sens. 33, 3768–3797.

Pu, R., Bell, S., Meyer, C., Baggett, L., Zhao, Y., 2012. Mapping and assessing seagrass along the western coast of Florida using Landsat TM and EO-1 ALI/Hyperion imagery. Estuar. Coast. Shelf Sci. 115, 234–245.

Purkis, S.J., Pasterkamp, R., 2004. Integrating in situ reef-top reflectance spectra with Landsat TM imagery to aid shallow-tropical benthic habitat mapping. Coral Reef. 23, 5–20.

Rohmann, S.O., Monaco, M.E., 2005. Mapping Southern Florida's Shallow-water Coral Ecosystems: an Implementation Plan. NOAA Technical Memorandum NOS NCCOS 19. NOAA/NOS/NCCOS/CCMA, Silver Spring, MD, p. 39.

Trimble, 2011. eCognition Developer 8.64.1 Reference Book.

Walker, B.K., 2009. Benthic Habitat Mapping of Miami-Dade County: Visual Interpretation of LADS Bathymetry and Aerial Photography. Florida DEP report #RM069. Miami Beach, FL, pp. 47.

Zapata-Ramírez, P.A., Blanchon, P., Olioso, A., Hernandez-Nuñez, H., Sobrino, J.A., 2013. Accuracy of IKONOS for mapping benthic coral-reef habitats: a case study from the Puerto Morelos Reef National Park, Mexico. Int. J. Rem. Sens. 34, 3671–3687.

Zhang, C., Xie, Z., 2012. Combining object-based texture measures with a neural network for vegetation mapping in the Everglades from hyperspectral imagery. Rem. Sens. Environ. 124, 310–320.

Zhang, C., Xie, Z., 2013a. Data fusion and classifier ensemble techniques for vegetation mapping in the coastal Everglades. Geocarto Int.. http://dx.doi.org/10.1080/10106049.2012.756940.

Zhang, C., Xie, Z., 2013b. Object-based vegetation mapping in the Kissimmee River watershed using HyMap data and machine learning techniques. Wetlands 33, 233–244.

Zhang, C., 2013. Applying data fusion techniques for benthic habitat mapping and monitoring in a coral reef ecosystem. ISPRS J. Photogramm. Rem. Sens. (submitted for publication).